PULSED POWER SYSTEMS FOR INERTIAL CONFINEMENT FUSION*

J. P. VanDevender

Sandia Laboratories

P. O. Box 5800
Albuquerque, New Mexico 87185

I. ABSTRACT

Sandia's Particle Beam Fusion Program is investigating pulsed electron and light ion beam accelerators with the goal of demonstrating the practical application of such drivers as igniters in inertial confinement fusion (ICF) reactors. The power and energy requirements for net energy gain are 10^{14}-10^{15} W and 1-10 MJ. Recent advances in pulsed power and power flow technologies permit suitable accelerators to be built. The first accelerator of this new generation is PBFA I. It operates at 2 MV, 15 MA, 30 TW for 35 ns and is scheduled for completion in June 1980. The principles of this new accelerator technology and their application to ICF will be presented.

II. INTRODUCTION

Thermonuclear fusion is the synthesis of light elements, such as deuterium into heavier elements like helium. In the process, a large amount of energy is released. Since we have a virtually unlimited supply of deuterium in our oceans, we have the potential of developing an unlimited energy source for commerical power production. This goal has encouraged research into controlled thermonuclear fusion for the past three decades. Most of that research has been directed towards magnetic confinement fusion, in which the hot dense plasma is confined in a magnetic bottle and the energy is slowly (0.1 s to 100 s) released. Excellent progress in that approach has been recently made. Another approach is to compress and heat the fuel so rapidly that it does not have time to expand, i.e., it is confined by its own inertia during the 10^{-8} to 10^{-9} s required for energy release. This approach is called inertial confinement fusion (ICF).

ICF is a power and energy intensive process. Powers of 10^{14} to 10^{15} watts and energies of 10^{6} to 10^{7} J are required. Until recently, the production of the power and energy pulse has been well beyond the capabilities of any laboratory source. However, technological advances in the past three years indicate that lasers, electron beams, light ion beams, and heavy ion beams can be constructed to provide the required power and energy for fusion. The development of an accelerator technology that can produce the necessary power and power density for ICF has been the goal of the Sandia Laboratories accelerator development program since 1970. The program has resulted in an accelerator technology that delivers electro-magnetic power at 34 TW/sr and is scalable to $> 10^{14}$ watts. The elements of the accelerator technology are the basic energy storage; module synchronization through gas dielectric switching; high-energy-density pulse-forming lines; short-pulse, water-dielectric switching, and long, self-magnetically insulated transmission lines for power transport to the diode. The system is reliable and is sufficiently flexible to accommodate both electron and ion beam generation for ICF experiments.

*This work was supported by the U.S. Dept. of Energy, under Contract DE-AC04-76-DP00789.

III. POWER PRODUCTION

Since the power requirements for ICF are many times the worlds power production capability, the energy in these accelerators must be slowly taken from the local power grid, stored in a large number of capacitors, and then temporally compressed through the pulse forming network. The temporal compression bridges the gap between the power consumption at 4×10^{9} W and the power production at $\sim 10^{14}$ W and is accomplished by modularization and synchronized switching. The total accelerator has been divided into modules, because the research and development costs are then minimized, the reliability is improved, and scalability to larger accelerators is assured. Each module of the accelerator technology is designed to deliver 0.8 TW of power for 35 ns at a power density of 34 TW/sr. The modules are synchronized by a triggered gap switch so all outputs can be simultaneously directed onto the target.

Each module produces its power by the stages illustrated in Fig. 1. The energy is stored in capacitors that are DC charged in parallel and then connected into a series configuration by spark gaps, represented by S1. Such a pulse forming network is called a Marx generator and is represented by a charged capacitor, an inductor, a resistor and a switch as shown in Fig. 1. Since the Marx is DC charged, the spacings between conductors are large to prevent electrical breakdown and cause the Marx inductance L to be large. The large inductance causes the energy transfer time to be ~ 600 ns.[1] The dimensions of the pulse forming line (PFL) are determined by the desired output pulse duration and risetime. Water is an excellent dielectric for high powered, pulse forming lines because of its high dielectric constant and cost effectiveness. Its breakdown strength and resistive losses are usually acceptable if the charge time is $\leq 1\ \mu s$. The stray capacities associated with trigger electrode structures in water are very large, and adequate trigger systems require too much energy. The switching of these state-of-the-art pulse forming lines must be accomplished with untriggered water switching.[2] The intrinsic jitter in the electrical breakdown process and the strong time dependence of the electrical breakdown strenth E_{BD} of water determine the risetime of the output power pulse. The 10 to 90 percent risetime of an output pulse[3] of voltage V_o into a matched impedance line is a strong function of the charge time and the voltage as shown in Figs. 2 and 3. Since ICF targets require 10 to 30 ns power

pulses with reasonably constant power levels, it is very desirable to limit the risetime to < 18 ns.

From Fig. 3 we see that the 1 μs charge time directly available from the Marx is too slow. Consequently, a low inductance transfer capacitor and a triggered gas switch S2 are used as shown in Fig. 1. The single extra stage decreases the charge time on the PFL to ~ 250 ns, which is adequate for $V_o \leq 1.5$ MV, as seen in Fig. 4. The triggered gas switch has a rms jitter of 1.8 ns and provides adequate synchronization between modules. The 1.5 MV output voltage is less than the 2.0 to 4.0 MV accelerating voltage that is desirable for various electron and light ion species, so transformers and/or stacked line techniques are used to increase the output voltage.

This modular pulsed power system has been developed and has been tested on the Mite and Hydramite modules at Sandia. In over four hundred shots at full power, the technology has been proven to be effective and reliable for generating power pulses for inertial confinement fusion particle accelerators.

IV. POWER FLOW

The pulse forming network produces power at a density of ~ 0.5 TW/m² and a power per unit solid angle of 34 TW/sr. The PFL is, therefore, located at a distance of 8 m from the target. The target requires power densities of 10^2 to 10^6 TW/m² so the power has to be spatially compressed during transport over 8 meters. The problem of transporting the power through the water, plastic, vacuum interface, and vacuum dielectrics to the diode is called the power flow problem. As the power flows through the elements of the "Power Flow Chain" as shown in Fig. 4, the electromagnetic power density must increase to ~ 10^4 W/m². The electromagnetic power can then be converted into particle beam power. An additional factor of 100 in the focused power density is requred to drive a target to ignition and may be achieved by beam focusing and multi-beam overlap techniques.

Each of these dielectrics has a characteristic breakdown strength that limits the power density through it, as shown by the boxes in Fig. 4. The weak link in the chain is the vacuum insulator, which has been the major obstacle to achieving larger accelerator output powers. Recently, the power flow problem has been solved. The low power density of the vacuum interface is accommodated by using a very large area of vacuum insulator divided among many modules. The approach necessitates transporting the power ~ 7 m to the target through vacuum at electrical stresses many times the conventional breakdown levels. The power transport to the vicinity of the target is accomplished through self-magnetically insulated transmission lines (MITL) as shown schematically in Fig. 5.

The self-magnetically insulated flow in a long MITL is established in the following steps as indicated in Fig. 6a-6d. When a voltage is applied to the parallel plate transmission line of impedance Z_o, a TEM wave propagates down the line as shown in Fig. 6a. When the electric field in the line reaches 25 to 40 MV/m, explosive emission[7] occurs on the cathode and a cathode plasma forms. A coating of carbon that is 2×10^{-5} m thick with a surface resistivity of 10^2 Ω/sq facilitates the formation of a spatially uniform cathode plasma. The plasma becomes a space charge limited source of electrons which are initially accelerated across the gap by the electric field, as shown in Fig. 6b. When the magnetic field from the displacement current density D and the electron loss current density J_l becomes *sufficiently large, the electrons* behind that point are prevented from reaching the anode and are magnetically insulated as shown in Fig. 6c. Since the conductance is greater than zero in the loss region, the region of loss propagates at a velocity less than c ≈ 3×10^8 m/s. Behind the lossy front, the pulse propagates at c.

As discussed by Kataev,[8] the effect is analogous to a shock wave in a gas. Since the shock velocity is less than the sound speed behind the front, the energy propagates to the shock front and steepens the pressure profile until the width of the shock front is determined solely by the nature of the dissipative process in the front. Similarly, the power flow to the lossy front in an "electromagnetic shock"[6] causes the voltage profile to steepen until it is limited by space-charge-limited electron flow in the front. In the Mite experiments,[6] the measured risetime of the front was limited by the frequency response of the Rogowskii coil current monitors and the recording oscilloscope to < 2 ns after six meters of line. When the voltage pulse has sharpened to its self-limited risetime, the structure propagates down the line as shown in Fig. 6d.

The structure of the front determines the ratio of the voltage and current behind the front and determines the sensitivity of the electron flow to perturbations in the line. The structure of the front has not been adequately investigated experimentally. However, the 2-D electromagnetic PIC simulations of Poukey and Bergeron[9] and the analytic theory of Gordeev[10] yield the following idealized model of the front as illustrated in Fig. 7. A voltage step, which has sufficient amplitude to form the cathode plasma, propagates down the line at the velocity of c. Since the lossy front propagates at a velocity $V_f < c$, the duration of this precursor increases with time. In the leading edge of the lossy front, the space-charge-limited electron emission loads down the voltage. Most of the loss current is lost at a voltage of 30 to 50 percent of V_o, which is the voltage behind the front.[9] Both the magnetic field and the voltage increase with increasing distance into the front. Behind the loss region, the vacuum gap between the electron flow and the anode increases with increasing distance from the front. As the electron flow recedes from the anode, the effective line impedance $\sqrt{L/C}$ increases and the voltage increases to V_o. The scale length over which the loss occurs is several times the gap width. Although the measurements of loss current density,[6] and precursor voltage[6,10-12] and pulse risetimes[6,10-12] are consistent with this model, the data has not been adequate to verify the details of the structure.

The details of the front structure are important because they determine the total current I_T and boundary current I_B (i.e., the current flowing in the metal, negative electrode) through the MITL behind the front. The 1-D theories[13-17]

have shown that the a continuum of solutions exists for the total current in a MITL at a given voltage. Each solution corresponds to a different value of I_T/I_B and a different boundary to the electron flow, as illustrated in Fig. 8 for parapotential[15] flow in a 2 MV line of impedance Z_o. The correct solution of the 1-D flow is determined by the 2-D flow in the front.

The experiments with short, self-limited lines and long self-magnetically insulated lines have shown that the ratio of $V_o/I_T Z_o$ is a function of the voltage.[5,18,19] These data are interpreted in Fig. 9 through the parapotential model to yield the ratio I_T/I_B and X_e/d_o in which X_e is the thickness of the electron flow and d_o is the vacuum gap. If $X_e/d_o = 1$, the electron flow entirely fills the vacuum gap and the flow is called saturated. If $X_e/d_o < 1$, the flow is unsaturated and there is a vacuum gap between the flow and the anode. The ratio of X_e/d_o indicates the sensitivity of the power transport to small perturbations in the gap separation. If the flow is very close to the anode, then small perturbations in the line geometry may cause the sheath to fluctuate and part of the flow to be lost. The parapotential model may not exactly describe the flow in a MITL, for example, the 2-D simulations[5] show that the sheath boundary is diffuse and is not discontinuous as the parapotential model requires. However, the location of the sheath boundary agrees with the model and, both experiments[6,10-12,17,18] and simulations[5] have shown sufficiently good agreement with the model to justify the utility of the model. We, therefore, conclude that the higher voltage MITL is less sensitive to gap tolerances and line perturbations, and efficient transport is more readily achieved at the higher voltages.

After considerable development of the technology, approximately 100 percent power transport and 90 percent energy transport efficiencies were achieved through a 6 m long, self-magnetically insulated transmission line.[6] The successful transport through the MITL completed the major pulsed power technology required by research accelerators for ICF.

Consequently, the technology is bounded by $V \leq 1.5$ MV for fast risetime water-dielectric switching and $V > 1.8$ MV for efficient power propagation through long self-magnetically insulated transmission lines. These two voltage requirements are bridged by using a transformer section.

V. PBFA I

The first accelerator of this generation is PBFA I, which is under construction at Sandia and is shown in Fig. 10. The accelerator consists of 36 synchronized modules and will deliver 3×10^{13} W of power at 2 MV and 15 MA for 35 ns to either an electron diode or ion diode located at 0.5 m from the target.

The operating sequence of each of the 36 modules begins with a 3.2 MV, 100 kJ Marx generator. The energy flows from the Marx into the 20 nF intermediate store capacitor in ≈ 600 ns. A gas insulated, triggered switch is then actuated to transfer the energy from the intermediate store capacitor to the water-insulated pulse forming line (PFL) in ≈ 250 ns. Untriggered, multichannel switching in the PFL then provides a 50 ns duration pulse with a 18 ns 10-90 percent risetime into the output pulse transformer and to the vacuum insulator. After passage through the vacuum insulator, one of the most inductive components in the accelerator, the power per unit area is increased to 500 TW/m^2 during transport through the magnetically insulated transmission line to the diode. The energy in the electromagnetic wave is then converted to particle beam energy by a diode. The particle beam is either guided to the target by a magnetized plasma column, which prevents beam dispersion, or ballistically focused to the target. Many beams are formed and then overlapped on the target to provide further power concentration.

It is evident from Fig. 10 that PBFA I utilizes only a small portion of the available solid angle around the target. If the available space were utilized, 400 TW and 16 MJ could be directed onto a target with today's technology. The accelerator can give experimental access to the high temperature and high density matter required for ICF and never before produced in a laboratory. Research on the accelerator will be directed towards developing the particle beam, ICF option for power production.

The high overall accelerator efficiency of ~25 percent and the low estimated cost of only \$40/J for a repetitively pulsed accelerator make power production through particle beam fusion attractive. The integration of the technology into a power reactor,[20] like the one shown schematically in Fig. 11, is directed towards the development of an experimental power reactor in the 1990's. The successful development of the accelerator technology for research into particle beam ICF encourages a degree of optimism that the remaining scientific and technical problems associated with an ICF reactor development will be overcome.

VI. ACKNOWLEDGEMENTS

I wish to gratefully acknowledge the helpful contributions from T. H. Martin of Sandia Laboratories in preparation of this paper and the members of the Pulsed Power Systems Department.

VII. REFERENCES

1. D. L. Johnson, Proc. Int'l. Pulsed Power Conf., Texas Tech University, Lubbock, TX, Paper IE2-1. (Nov. 9-11, 1976).
2. J. P. VanDevender and T. H. Martin, IEEE Trans. Nucl. Sci. NS-22, 979 (1975).
3. J. P. VanDevender, Electron Beam Fusion Progress Report, Jan.-June 1979, Sandia Laboratories, Albuq., NM.
4. T. P. Wright, J. Appl. Phys. 49, 3842 (1978).
5. K. D. Bergeron and J. W. Poukey, Appl. Phys. Lett. 32, 8 (1978).
6. J. P. VanDevender, J. Appl. Phys. 50, No. 7 (June 1979).
7. G. A. Mesyats and D. I. Proskurovskii, JETP Lett. 13, 4 (1977).
8. I. G. Kataev, Electromagnetic Shockwaves (in Russian), Sov. Radio Moscow (1963); (in English) Iliffe Books, Ltd., London (1966).
9. A. V. Gordeev, Sov. Phys.-Tech. Phys. 23, 991 (1978).
10. I. D. Smith, P. D'A.Champney and J.M.Creedon, IEEE Pulsed Power Conf., Lubbock, TX (1976).

11. E. I. Baranchikov, A. V. Gordeev, V.D.Korolev and V. P. Smirnov, Sov. Phys.-Tech. Phys. 8, 42 (1977).
12. M. DiCapua and D. G. Pellinen, J. Appl. Phys. 50, (1979).
13. W. V. Lovelace and E. Ott, Phys. Fluids 17, 1263 (1974).
14. A. Kon, A. A. Mondelli and N. Rostoker, IEEE Trans. Plasma Sci. PS-1, 85 (1973).
15. J. M. Creedon, J. Appl. Phys. 46, 2946 (1975) and J. M. Creedon, J. Appl. Phys. 48, 1070 (1977).
16. V. S. Veronin and A. I. Lebedev, Sov. Phys.-Tech. Phys. 18, 1627 (1974).
17. C. W. Mendel, Accepted for publication in J. Appl. Phys. 50, No. 7, (July 1979).
18. S. Shope, J. W. Poukey, K. D. Bergeron, D.H.McDaniel, A.L.Toepfer and J.P.VanDevender, J. Appl. Phys. 49, 3675 (1978).
19. A. A. Kolomenskii, E. G. Krastelev and B. N. Yablokov, Sov. Phys.-Tech. Phys. 3, 247 (1977).
20. D. L. Cook and M. A. Sweeney, Proc. of the 3rd ANS Topical Mtg. on the Tech. of Controlled Nucl. Fusion, Santa Fe, NM (May 9-11, 1978).

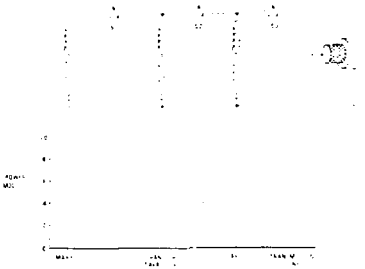

Fig. 1. Power production through staged, synchronized switching.

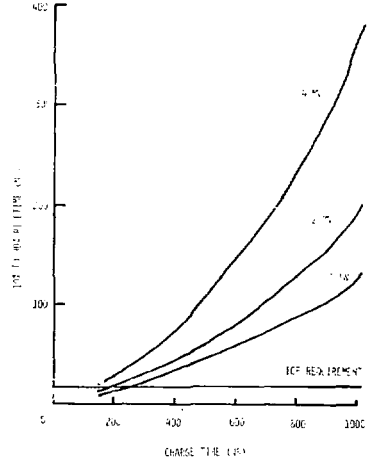

Fig. 2. The risetime of the output pulse as a function of the PFL charge time for output voltages of 1, 2, and 4 MV into a matched load.

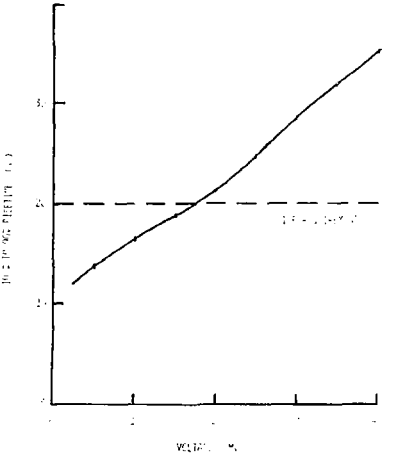

Fig. 3. The risetime of the output pulse vs. the output voltage into a matched load for a 250 ns charge time.

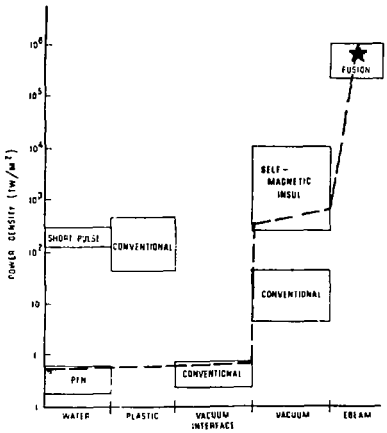

Fig. 4. The power flow chain. The chosen path is shown by the dashed line.

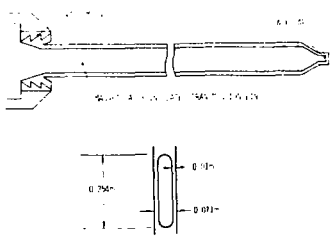

Fig. 5. Schematic diagram of a EBFA magnetically insulated transmission line.

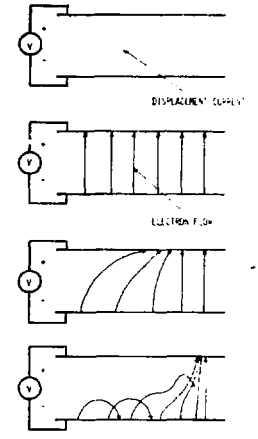

Fig. 6. The stages by which self-magnetically insulated flow is established in a MITL.

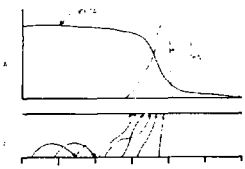

Fig. 7. The structure of the front in a MITL. The voltage and loss current density are shown in A and the electron map is shown in B. The pulse risetime is ~0.3 ns.

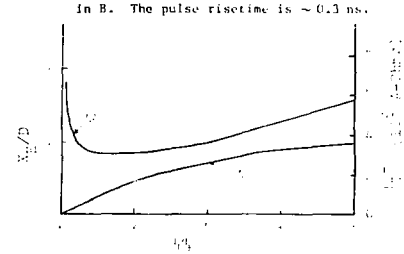

Fig. 8. The range of solutions of total current I_T and electron sheath thickness X_E in a MITL with impedance Z_0, gap separation D and voltage 2.0 MV from parapotential theory. I_T/I_B is the ratio of the total and boundary currents.

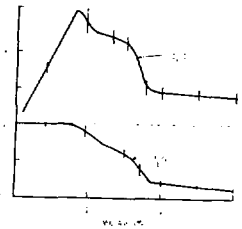

Fig. 9. The ratio of total current I_T to boundary current I_B vs voltage V has been inferred from experimental data of I_T (V). The normalized sheath position X_E/D that corresponds to I_T/I_B is also shown. At low voltages the electrons fill the gap.

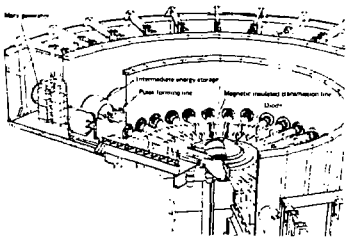

Fig. 10. Schematic diagram of PBFA I.

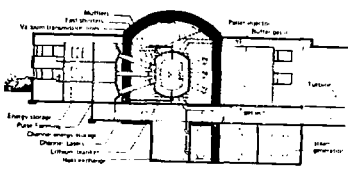

Fig. 11. Schematic diagram of a fusion reactor based on particle beam fusion.